The Location of an Engineered Inter-Subunit Disulfide Bond in Factor for Inversion Stimulation (FIS) Affects the Denaturation Pathway and Cooperativity†

Derrick Meinhold,‡ Michael Beach,|| Yongping Shao,§ Robert Osuna,§ and Wilfredo Colón*,‡

Department of Chemistry and Chemical Biology, Rensselaer Polytechnic Institute, 110 8th Street, Troy, New York 12180, Department of Biological Sciences, State University of New York at Albany, 1400 Washington Avenue, Albany, New York 12222, and Department of Biology, Chemistry, and Physics, Southern Polytechnic State University, 1100 South Marietta Parkway, Marietta, Georgia 30060

Received April 5, 2006; Revised Manuscript Received June 7, 2006

ABSTRACT: Two crossed-linked variants of the homodimeric DNA binding protein factor for inversion stimulation (FIS) were created via engineering of single intermolecular disulfide bonds. The conservative S30C and the nonconservative V58C FIS independent mutations resulted in FIS crossed-linked at the A helix (C30−C30) and at the middle of the B helix (C58−C58). This study sought to investigate how the location of an intermolecular disulfide bond may determine the effect on stability and its propagation through the structure to preserve or alter the denaturation cooperativity of FIS. The oxidized and reduced S30C and V58C FIS exhibited a far-UV CD spectrum and DNA binding affinities that were similar to WT FIS, indicating no significant changes in secondary and tertiary structure. However, the reduced and oxidized forms of the mutants revealed significant differences in the stability and equilibrium denaturation mechanism between the two mutants. In the reduced state, S30C FIS had very little effect on FIS stability, whereas V58C FIS was 2−3 kcal/mol less stable than WT FIS. Interestingly, while both disulfide bonds significantly increased the resistance to urea- and guanidine hydrochloride (GuHCl)-induced denaturation, oxidized V58C FIS exhibited a three-state GuHCl-induced transition. In contrast, oxidized S30C FIS displayed a highly cooperative WT-like transition with both denaturants. The three-state denaturation mechanism of oxidized V58C FIS induced by the GuHCl salt was reproduced by urea denaturation at pH 4, suggesting that disruption of a C-terminus salt-bridge network is responsible for the loss of denaturation cooperativity of V58C FIS in GuHCl or urea, pH 4. A second mutation on V58C FIS created to place a single tryptophan probe (Y95W) at the C-terminus further implies that the denaturation intermediate observed in disulfide crossed-linked V58C FIS results from a decoupling of the stabilities of the C-terminus and the rest of the protein. These results show that, unlike the C30−C30 intermolecular disulfide bond, the C58−C58 disulfide bond did not evenly stabilize the FIS structure, thereby highlighting the importance of the location of an engineered disulfide bond on the propagation of stability and the denaturation cooperativity of a protein.

The engineering of disulfide bonds into monomeric proteins has shown that the incorporation of a well-placed disulfide bond has the potential to significantly increase protein stability (*1*−*10*). This effect has been attributed to thermodynamic factors, such as a decrease in conformational entropy of the unfolded state (*11*), an enthalpic effect on the native state (*5*), and a greater preference for the burial of a disulfide group over burial of two reduced cysteine residues (*10*). The most widely applied mathematical models for calculating the effect of a disulfide bond on the conformational entropy change of a monomeric polymer are (1) $\Delta S = -2.1 - {}^3/_2 R(\ln n)$ (*2*) (for a single cross-link), where n is the number of amino acids in the loop created by the cross-link, and (2) $\Delta S = k\upsilon[{}^9/_8 \ln(\upsilon/N) - 3.4]$ (*11*) (for multiple cross-links), where k is the Boltzmann constant, υ is the number of cross-links, and N is the number of statistical units (amino acids) in the chain. Based on these equations, the entropic stabilization by cross-linking a single polypeptide chain is derived solely from the length of the chain, the number of cross-links, and most importantly, the size of the loop created by the cross-link. However, when considering the entropic effect of a single engineered intermolecular disulfide bond in a dimeric protein, these equations do not adequately explain the entropic effect because no loops are created. Furthermore, the location of the disulfide bond could lead to different chain topologies, ranging from the formation of a long linear chain (e.g., cross-linking between both termini) to the formation of a branched chain (e.g., cross-linking at the middle of the chain).

There are numerous examples of studies that describe the effect of intramolecular disulfide bonds on the cooperativity of equilibrium denaturation (*1*, *4*, *8*, *12*−*14*). For example, the incorporation of a disulfide bond in dihydrofolate

† This work was supported by grants from the National Science Foundation (Grant NSF MCB-9984913) to W.C. and from the National Institutes of Health (Grant GM52051) to R.O.

* To whom correspondence should be addressed. E-mail: colonw@rpi.edu. Phone: (518) 276-2515. Fax: (518) 276-4887.

‡ Rensselaer Polytechnic Institute.

|| Southern Polytechnic State University.

§ State University of New York at Albany.

10.1021/bi060672n CCC: $33.50
Published on Web 07/25/2006

reductase resulted in a decrease in denaturation cooperativity compared with that of the reduced protein, suggesting the formation of an equilibrium denaturation intermediate (*8*). In some cases, a decreased cooperativity of the disulfide-linked protein was attributed to residual structure in the unfolded state, while in other instances, it appeared to be caused by the marginal population of intermediates.

Few experimental and theoretical studies have been carried out to understand the effects of intermolecular disulfide cross-links on protein stability and denaturation cooperativity (*12*, *15*−*17*). In most cases, intermolecular disulfide bonds have been engineered in dimeric proteins, and the effect has been mainly to increase the stability of the protein. For example, an engineered solvent-exposed intersubunit disulfide bond in the homodimeric Arc repressor protein resulted in an increase in T_m and C_m, but there was no change in the denaturation cooperativity (*17*). In another case, the N-terminal domain of the λ phage repressor protein was engineered to form two mutants with a single disulfide cross-link bridging the dimer interface. One disulfide bond reduced the stability below that of the WT protein, whereas the other significantly stabilized the protein. However, neither caused any detectable change in the denaturation cooperativity (*15*). Interestingly, when the location of an engineered disulfide bond was changed, as in the case of a homodimeric four-helix bundle, there were small differences in the cooperativity of the GuHCl denaturations (*16*). The *m*-values were shown to differ between the oxidized and reduced forms of the proteins, and the authors attributed this effect to non-two-state behavior. Thus, engineering disulfide bonds across protein interfaces is more likely to increase protein stability without affecting the equilibrium denaturation cooperativity.

In this study, we have used the homodimeric protein factor for inversion stimulation (FIS),[1] a bacterial nucleoid-associated protein, as a model system to understand how the presence and location of an intermolecular disulfide bond may affect the stability and denaturation cooperativity of a dimeric protein. Also, it was of interest to design a cross-linked version of FIS that could be used to examine the effect of FIS stability and dissociation on the function of this protein, since previous studies showed that FIS readily dissociates in solution at concentrations well above those required for specific DNA binding (*18*, *19*). Thus, we engineered two separate cysteine mutations, S30C and V58C, each of which can form an intermolecular disulfide bond with the same cysteine residue (e.g., C30−C30 or C58−C58) in the opposite chain. We tested the effects of each disulfide bond on the stability and denaturation cooperativity of FIS via urea- and GuHCl-induced denaturation in both the oxidized and reduced forms and found very different effects by each disulfide bond. The denaturation of S30C FIS revealed a cooperative two-state denaturation mechanism and stability similar to WT FIS. In contrast, the denaturation of V58C FIS revealed the population of an intermediate, and further experiments showed that the intermediate contains a disrupted C-terminal DNA-binding subdomain. Thus the presence of a C58−C58 disulfide bond leads to the accumulation of an equilibrium denaturation intermediate due to differential stabilization of subdomains within FIS, whereas the C30−C30 disulfide bond propagates its stabilizing effect homogeneously throughout the structure of FIS. These observations demonstrate that the precise location of an intersubunit disulfide bond in FIS can have very different effects on the stability and denaturation cooperativity.

[1] Abbreviations: AA, amino acid; CD, circular dichroism; far-UV, far ultraviolet; FIS, factor for inversion stimulation; V58C, valine to cysteine mutation at position 58; S30C serine to cysteine mutation at position 30; PB, phosphate buffer; SDS−PAGE, sodium dodecyl sulfate−polyacrylamide gel electrophoresis; WT, wild-type.

MATERIALS AND METHODS

Protein Expression, Purification, and Preparation. The V58C mutation was constructed and sequenced as previously described with a two-step PCR method (*18*), while the S30C and V58C/Y95W mutations were prepared using the Quick Change II Kit (Stratagene) and sequenced by the Center for Functional Genomics (Albany, N. Y.). WT and the cysteine-mutant FIS sequences were overexpressed in *Escherichia coli* and purified by running two sequential SP Sepharose cation exchange columns. FIS was removed from the column using a 0.3−1.0 and 0.4−0.6 M NaCl gradient for the first and second columns, respectively, resulting in >95% pure FIS according to sodium dodecyl sulfate polyacrylamide gel electrophoresis (SDS−PAGE) and reversed-phase HPLC. The concentration of FIS was determined in FIS monomer units by measuring the absorbance at 276 nm in 8 M GuHCl and using extinction coefficients of 5820, 5980, and 9930 M^{-1} cm^{-1} for WT FIS, disulfide-bonded FIS, and disulfide-bonded V58C/Y95W FIS, respectively (*20*). All experiments were performed in 10 mM phosphate buffer (PB) at pH 7.4 with 0.1 M NaCl at 20 °C, except for the low pH urea denaturation experiments for which HCl was added to lower the pH to 4.0. Disulfide bond formation was nearly 100% for both mutants and occurred immediately upon purification for V58C FIS, while S30C FIS required ∼78 h of incubation at 4 °C at 0.5 mM FIS (monomer concentration). The formation of a disulfide cross-linked dimer was verified using SDS−PAGE (in the absence of a reducing agent) and reversed-phase HPLC. Reduction of ∼0.2 mM FIS cysteine mutants was accomplished with 50 mM DTT and 6 M urea or 4 M GuHCl at 25 °C. Dilution of these reduced samples facilitated preparation of refolded/reduced and unfolded/reduced protein stocks that were used in this work. The reduced samples (made with freshly prepared DTT) were analyzed immediately upon refolding to minimize the accumulation of oxidized species. Calculation of the amount of DTT, denaturant, and protein added to the concentrated, unfolded reduction mixture was dependent on the desired conditions of the final diluted volumes used for experimentation (see below).

FIS Denaturation Monitored by Circular Dichroism. Equilibrium denaturation experiments monitored by circular dichroism (CD) were performed on an OLIS CD instrument (Bogart, Georgia) with 1.8 μM FIS in a cuvette with a 1 cm path length, while CD wavelength scans were performed with 36 μM FIS in a light path length of 1 mm. To examine the protein concentration dependence of the transitions, experiments at 8.9 μM FIS (data not shown) were compared with those at 1.8 μM FIS.

The equilibrium denaturation experiments were accomplished by measuring the ellipticity at 222 and 255 nm before extracting a portion of the folded sample from the cuvette

and replacing it with an equal volume of an unfolded protein stock (10 M urea or 8 M GuHCl) of identical protein concentration. Before subsequent data collection, samples were allowed to equilibrate (less than 1 min) until a time-dependent signal change was no longer noticed. The sample that was extracted from the cuvette was applied to a Reichert refractometer (Depew, NY) to determine the refractive index of the sample, which was then used to calculate the exact concentration of denaturant for each data point. The CD signal at 255 nm was subtracted from the signal at 222 nm as a baseline control. Repetition of this titration procedure systematically increased the concentration of denaturant in the cuvette.

For equilibrium denaturation experiments of the proteins with reduced cysteines, both the folded and the unfolded stocks were made by diluting the reduced/unfolded samples as described above in either refolding buffer or concentrated denaturant. It was necessary to dilute the DTT in both samples to a concentration of less than 2 mM to avoid significant UV absorbance, which prevents ellipticity measurement. The folded stock was refolded by dilution with 10 mM phosphate buffer (pH 7.4) and 0.1 M NaCl, whereas the unfolded stock was diluted with 10 M urea or 8 M guanidine (dissolved in 10 mM phosphate buffer and 0.1 mM NaCl). In preparing the refolded stock via dilution, it was necessary to start with a small volume of unfolded/reduced protein in which the protein was sufficiently concentrated to allow adequate dilution of denaturant (final concentration of <0.5 M urea or <0.1 M GuHCl), while maintaining a final protein concentration of 1.8 μM.

Full reversibility of the denaturation transitions was confirmed by observing identical far-UV CD signal of folded and refolded samples of each protein. In addition, no time-dependent change in the CD signal was noticed after the 1 min equilibration period for the points along the transition of each protein. Finally, all the urea and GuHCl denaturation curves were internally normalized based on the fraction of native signal loss as follows: (signal $-$ signal$_{folded}$)/($-$signal$_{folded}$). This method of normalization allows for comparison of the degree of unfolding completed between each protein/denaturant combination used in this study.

Denaturation of V58C/Y95W FIS Monitored by Tryptophan Fluorescence. One tryptophan mutation (Y95W) was incorporated into V58C FIS to allow us to study the environment and stability of the C-terminus of oxidized (disulfide-bonded) V58C FIS. The fluorescence-monitored equilibrium denaturation experiment of this mutant was performed on a Hitachi spectrofluorimeter using the codilution method explained above. The tryptophan was excited at 295 nm, and emission wavelength scans were recorded from 320 to 380 nm. Since the change in fluorescence intensity between 0 and 3 M GuHCl was not significant, we use the shift in the maximum fluorescence wavelength to monitor the denaturation transition. The broad fluorescence band makes it difficult to accurately determine the fluorescence maxima, so we determined the wavelength of maximum fluorescence by fitting the emission spectra to the cubic polynomial ($y = ax^3 + bx^2 + cx + d$) in Excel where y is signal intensity and x is wavelength. The cubic polynomial was the lowest order polynomial that fit the fluorescence emission spectra well and allowed calculationof the wavelength of maximum signal via the x intercept of its first derivative:

$$\lambda_{\text{max fluorescence}} = \frac{-2b - \sqrt{4b^2 - 12ac}}{6a} \quad (1)$$

The coefficients derived from the cubic fit to each emission wavelength scan were used in eq 1 to calculate the wavelength (λ) of maximum fluorescence.

Analysis of Denaturation Data. The denaturation transitions were analyzed using KaleidaGraph, version 3.51 (Synergy software). The data for WT and reduced form of the cysteine mutants were fit to a two-state ($N_2 \leftrightarrows 2U$) model involving the native dimer and unfolded monomer, using the equation

$$Y = Y_N(1 - F_U) + Y_U F_U \quad (2)$$

where the signal, Y, is equal to the fraction unfolded (F_U) plus fraction native ($1 - F_U$) multiplied by the native (Y_N) and unfolded (Y_U) signals, which vary linearly with denaturant concentration. To obtain the thermodynamic parameters, F_U was defined in terms of the equilibrium constant for unfolding (K_U) and the total monomer concentration (Pt) by combining the equations $K_U = [U]^2/[N_2]$, $Pt = 2[N_2] + [U]$, and $F_U = [U]/Pt$ to obtain the following equation (*21*):

$$F_U = \frac{-K_U + \sqrt{K_U{}^2 + 8K_U Pt}}{4Pt} \quad (3)$$

The equilibrium denaturations of the oxidized FIS mutants that displayed single cooperative transitions were appropriately fit to a two-state mechanism ($N_2 \leftrightarrows U_2$), which accounts for cross-linked unfolded and folded states. The instrumental signal for this mechanism is expressed in the same way as for the two-state mechanism involving a monomeric unfolded state (eq 2), while the fraction unfolded is expressed as

$$F_U = \frac{K_U}{1 + K_U} \quad (4)$$

Equation 4 also served to model the F_U for the ($N_2 \leftrightarrows I_2$) curve fit in Figure 5.

Some of the oxidized cysteine mutant denaturation data showed obvious decoupling between two separate transitions and thus were fit to a three-state ($N_2 \leftrightarrows I_2 \leftrightarrows U_2$) mechanism. The instrumental signal (Y) was fitted to the equation

$$Y = Y_{N_2}(1 - F_{U_2} - F_{I_2}) + Y_{I_2}F_{I_2} + Y_{U_2}F_{U_2} \quad (5)$$

where (F_{U_2}), (F_{I_2}), and (F_{N_2}) are the fraction unfolded, intermediate, and native dimer, respectively. The definition of F_U for the three-state mechanism ($N_2 \leftrightarrows I_2 \leftrightarrows U_2$) is

$$F_U = \frac{1}{1 + \frac{1}{K_2} + \frac{1}{K_2 K_1}} \quad (6)$$

in which K_1 and K_2 are the equilibrium constants for the $N_2 \leftrightarrows I_2$ and $I_2 \leftrightarrows U_2$ transitions, respectively.

Equilibrium constants were then defined in terms of ΔG of unfolding, denaturant (D) concentration, and m-value ($\delta\Delta G/\delta D$) based on the linear extrapolation model of protein

stability ($\Delta G_{H_2O} = \Delta G - mD$) and the universal relationship between K_{eq} and ΔG, $\Delta G = -RT \ln(K_{eq})$.

$$K_U = \exp\left(\frac{-\Delta G_{H_2O} + mD}{RT}\right) \quad (7)$$

ΔG_{H_2O} is protein stability in the absence of denaturant, and D is the concentration of denaturant. The m-value correlates with the amount of buried surface that becomes exposed upon unfolding (*22*). Although the expression for $F_U(K_U)$ differs based on the denaturation mechanism, the $K_U(\Delta G)$ expression remains constant regardless of the model.

DNA Binding Assay. The DNA-binding affinities of each of the FIS mutants in their reduced or oxidized forms were compared with that of the WT protein using the gel electrophoretic mobility shift assay, as previously described (*19*). Various concentrations of FIS were mixed with a 42 bp ^{32}P-labeled DNA fragment containing an engineered high-affinity symmetrical FIS DNA binding sequence (GCT-CAAATTTTGAGC) in 20 μL of binding buffer (20 mM Tris-HCl [pH7.5], 10 mM EDTA, 80 mM NaCl), incubated at room temperature for 10 min, and combined with 5 μL of loading buffer (20 mM Tris-HCl [pH7.5], 10 mM EDTA, 80 mM NaCl, 100 μg/mL sonicated salmon sperm DNA, 7.5% Ficoll, 0.1% bromophenol blue). Samples were then loaded onto an 8% polyacrylamide/bisacrylamide (60:1) gel in TBE buffer (0.089 M Tris-borate [pH 8.3], 2.5 mM EDTA) with a 15-mA conducting current. The relative signal intensities of the bound and unbound DNA were quantified by phosphorimaging, and the FIS concentration required to achieve 50% binding was taken as an approximation of the K_d (apparent K_d).

RESULTS

Structural Environment of Ser30 and Val58. Inspection of the X-ray crystal structure of WT FIS (*23*, *24*) revealed two different amino acids, Ser30 and Val58, that are in close proximity to the same residue on opposite subunits and therefore appeared to be good sites for the incorporation of intermolecular disulfide bonds (Figure 1A). In WT FIS, Ser30 is exposed to the solvent and the α-carbon distance between Ser30 in the A and B chains is about 7.2 Å (Figure 1B). In the case of Val58, the distance between the α-carbon atoms is 8.0 Å, and the side chains are buried, interacting hydrophobically with one another and with the surrounding residues Val54, Val31, and Leu27 (Figure 1C). The α-carbon distances of Ser30 and Val58 across the subunits are greater than the average separation in native disulfide bonds, of which only 6% have an α-carbon distance greater than 6.6 Å and none have a distance greater than 7.4 Å in comparison to a dataset in ref *25*.

Structural and Functional Effects of the S30C and V58C Mutations. Both the S30C and V58C FIS mutants formed the expected intermolecular disulfide bond upon incubation at 4 °C and pH 7.4 at 0.5 mM protein monomer concentration, demonstrating that these residues are near each other and in the proper orientation, as anticipated based on the WT FIS crystal structure. The far-UV CD spectra of oxidized and reduced S30C and V58C FIS were virtually identical to that of WT FIS (Figure 2A), indicating no major disruption of secondary structure. Neither the S30C nor the V58C

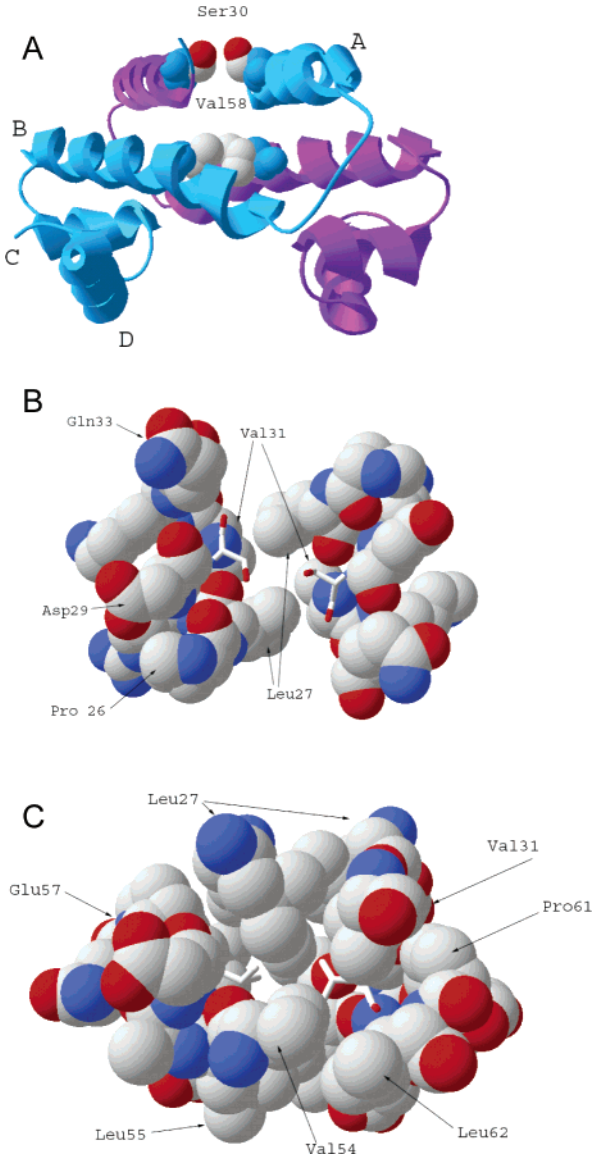

FIGURE 1: (A) The X-ray crystal structure of WT FIS (PDB file 3FIS) residues 27−98. Residues 1−26 are flexible and do not resolve in the crystal structure. The residues at position 30 and 58, which were separately mutated to cysteine, are highlighted in spacefill. The four α helices in the protein are labeled A−D. (B) Close-up of the region within 5 Å of Ser30 reveals that side chain 30 is in a solvent exposed cleft at the intermolecular interface between the two A helices. (C) Close-up of the region within 5 Å of Val58 shows that it is buried and involved in numerous hydrophobic interactions at the dimer interface that bridge the two B helices, as well as the B and A helices. This figure was prepared using the program Deep View Swiss PDB Viewer (*51*).

mutations in their oxidized forms disrupted the ability of FIS to bind to a specific site on the DNA. In fact, these mutations resulted in a moderate decrease in the apparent K_d compared with WT FIS, suggesting a small increase in the DNA binding affinity (Table 1). The reduced forms of these mutants also bound DNA with higher affinity than WT FIS, although with slightly lower K_d values than the oxidized forms. These results indicate that the incorporation of a disulfide bond at positions 30 and 58 does not disrupt the structure or DNA binding function of FIS. Moreover, cross-linking the subunits of FIS with disulfide bridges did not appear to confer a functional advantage.

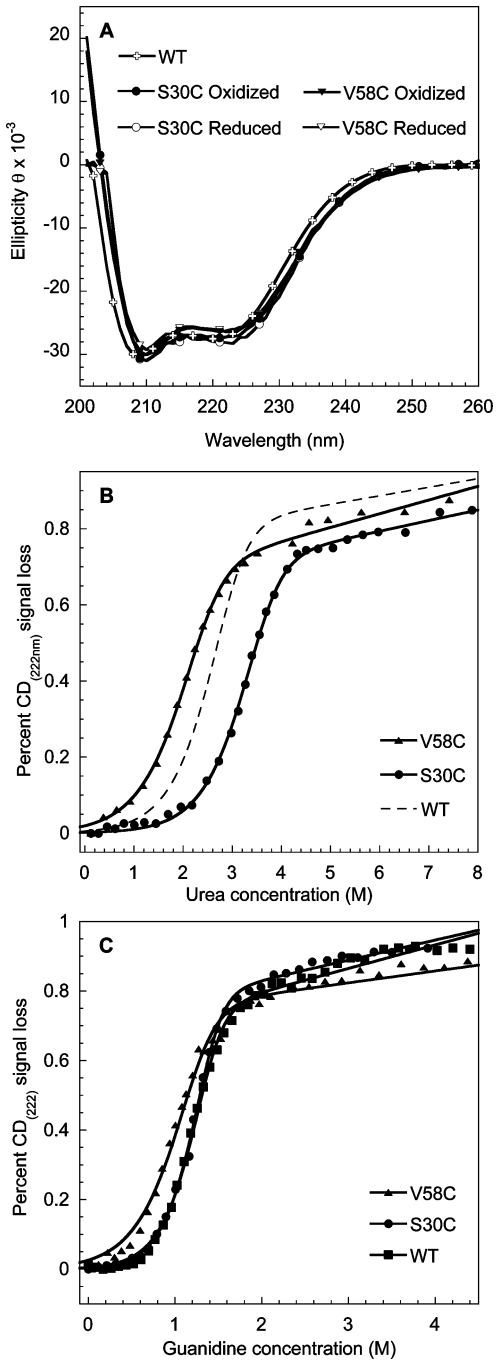

FIGURE 2: (A) Far-UV CD wavelength scans of WT FIS and the oxidized and reduced forms of the V58C and S30C mutants. (B) CD-monitored urea denaturations and (C) GuHCl denaturations of WT FIS and the reduced forms of V58C and S30C FIS. The solid line curve fits in panels B and C are based on the $N_2 \leftrightarrows U_2$ equilibrium mechanism defined in the Materials and Methods. Data in panels B and C were normalized by percent signal change (Y) from the first point (F): $Y = (\text{signal} - F)/Y$.

Equilibrium Denaturation of Reduced S30C and V58C FIS. To determine the intrinsic effect of the S30C and V58C mutations on the thermodynamic stability of FIS, we carried out urea and GuHCl equilibrium denaturation experiments on the reduced protein and monitored the transition using far-UV CD. The urea and GuHCl data were in good agreement with a ΔG value that was the same for V58C FIS, but for WT and S30C FIS, it was 1.2−1.6 kcal/mol higher in the case of urea denaturation. Interestingly, S30C FIS has a higher urea-induced denaturation midpoint (C_m) than WT FIS, but the ΔG was almost the same due to a compensatory small decrease in m-value (Figure 2B, Table 2). V58C FIS had a lower C_m and m-value than WT FIS, resulting in about 2−3 kcal/mol lower stability (Table 2, Figure 2B). The notably decreased m-values of reduced V58C, compared with the WT protein, may be caused by the small pretransition baselines, which make fitting less accurate, or by the possible presence of a small percentage of oxidized protein in the sample, which would broaden the transition. The hydroxyl side chain of Ser30 is highly solvent exposed and has little potential for hydrogen bonding aside from a possible interaction between the hydrogen from the hydroxyl of one side chain to the oxygen electron lone pair of the opposite chain serine. In contrast, Val58 is involved in substantial nonpolar interactions in the hydrophobic core of FIS.

Table 1: Relative DNA Binding Activities of WT, S30C, and V58C FIS

FIS	K_d (nM)[a]
WT	0.081 ± 0.007
S30C reduced	0.018 ± 0.001
S30C oxidized	0.035 ± 003
V58C reduced	0.046 ± 0.004
V58C oxidized	0.062 ± 0.004

[a] Apparent K_d values and standard deviations are given as an average of at least three independent assays.

Table 2: Equilibrium Denaturation Analysis of WT FIS and Reduced Cysteine Mutants[a]

protein	denaturant	$\Delta G_{N_2 \leftrightarrow 2U}$ (kcal/mol)	$m_{N_2 \leftrightarrow 2U}$ (kcal/(mol·M))
WT[b]	urea	14.7 ± 1.7	2.4 ± 0.1
WT	GuHCl	13.1 ± 0.2	4.7 ± 0.2
S30C reduced	urea	14.0 ± 0.2	2.0 ± 0.1
S30C reduced	GuHCl	12.8 ± 0.2	3.9 ± 0.7
V58C reduced	urea	11.0 ± 0.1	1.8 ± 0.1
V58C reduced	GuHCl	11.3 ± 0.2	3.5 ± 0.2

[a] Denaturations of the reduced cysteine mutants and WT FIS were fit to a $N_2 \leftrightarrows 2U$ denaturation mechanism. Errors are the standard deviations based on three independent experiments. [b] Data and fitting of WT urea denaturation is as previously described (*28*).

Equilibrium Denaturation of Oxidized S30C and V58C FIS. Oxidation of S30C and V58C FIS to yield a disulfide cross-linked protein occurred spontaneously upon purification and was verified by reverse-phase HPLC and the appearance of a single band with dimer MW in SDS−PAGE. Oxidation of V58C FIS was close to 100% immediately after purification, whereas S30C required about 72 h of incubation at 4 °C to achieve full oxidation at pH 8.5 (data not shown). The equilibrium denaturation of oxidized S30C FIS in urea and GuHCl were cooperative and had significantly higher C_m's, but lower m-values than WT FIS when fitted to a two-state unimolecular model (Figure 3).

Oxidized V58C FIS showed less cooperativity than either WT or S30C FIS when unfolded in GuHCl or urea. The two-state model ($N_2 \leftrightarrows U_2$) fits of the urea denaturation transition yielded an unexpectedly low m-value and ΔG (Table 3). Such low m-value and ΔG, in comparison with the GuHCl results, are likely attributed to the formation of an intermediate, although the m-value is lowered by the considerable slope of the post-transition baseline. Surprisingly, the GuHCl denaturation of V58C FIS resulted in a biphasic transition,

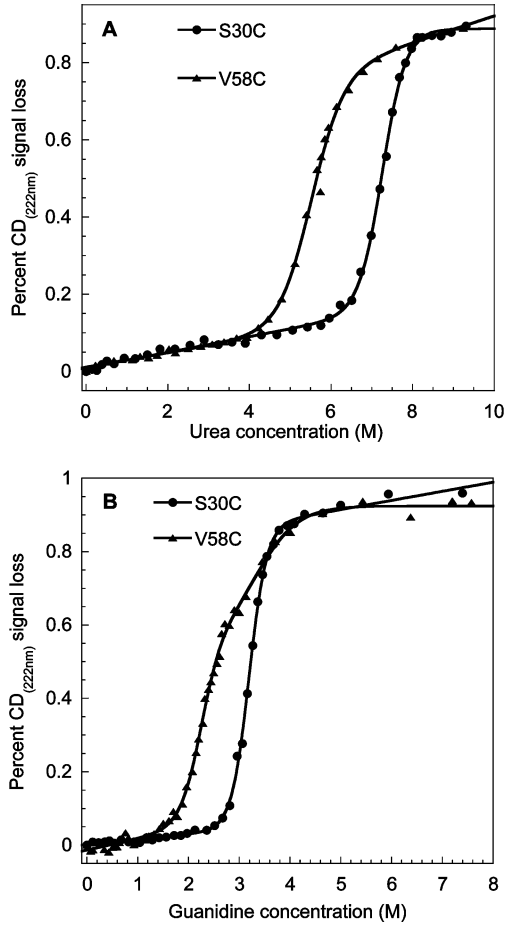

FIGURE 3: Far-UV CD monitored (A) urea and (B) GuHCl denaturations of oxidized V58C and S30C. The solid line in the V58C FIS data in panel B is a curve fit based on the $N_2 \leftrightarrows I_2 \leftrightarrows U_2$ equilibrium pathway, and all other curve fits in both panels are based on the pathway $N_2 \leftrightarrows U_2$. Data were normalized as in Figure 2.

Table 3: Equilibrium Denaturation Analysis of the Oxidized Cysteine Mutants

protein	denaturant	ΔG (kcal/mol)	m [kcal/(mol·M)]	fit to the unfolding pathway
S30C	urea	13.7 ± 0.7	1.9 ± 0.1	$N_2 \leftrightarrows U_2$
S30C	GuHCl	11.0 ± 0.4	3.5 ± 0.1	$N_2 \leftrightarrows U_2$
V58C	urea	6.7 ± 0.6	1.2 ± 0.1	$N_2 \leftrightarrows U_2$
V58C	GuHCl	10.3 ± 1.7[a]	3.9 ± 0.5a	$N_2 \leftrightarrows I_2 \leftrightarrows U_2$

[a] Oxidized V58C denaturation via GuHCl yielded an obvious three-state denaturation mechanism, and thus it was possible to fit the single denaturation curve to a three-state ($N_2 \leftrightarrows I_2 \leftrightarrows U_2$) mechanism. The results for each transition were resolved. For $N_2 \leftrightarrows I_2$, $\Delta G = 5.8$ kcal/mol and m-value = 2.6 kcal/(mol·M), and for $I_2 \leftrightarrows U_2$, $\Delta G = 4.5$ kcal/mol and m-value = 1.3 kcal/(mol·M). Errors are the standard deviations based on three independent experiments.

which was fitted to a three-state denaturation model ($N_2 \leftrightarrows I_2 \leftrightarrows U_2$) to obtain the ΔG's and m-values for the two unfolding transitions (see footnote in Table 3). The difference in stability of oxidized V58C FIS obtained in urea and GuHCl suggests that despite the two-state-like transition observed in urea, the denaturation mechanism may be more complex. When an intermediate is marginally populated, even if the transition appears two-state, fitting the data to a two-state model can dramatically underestimate the resulting ΔG. Thus, the denaturation of oxidized V58C FIS appears to involve the population of an intermediate, and the decoupling of the V58C FIS transitions in GuHCl but not in urea indicates that each denaturant has a different effect on the equilibrium denaturation pathway of V58C FIS. Different degrees of transition decoupling by the two denaturants are likely due to a localized sensitivity of FIS to the charged nature of GuHCl, resulting in a denaturation efficiency that is not uniform throughout the crossed-linked V58C FIS structure.

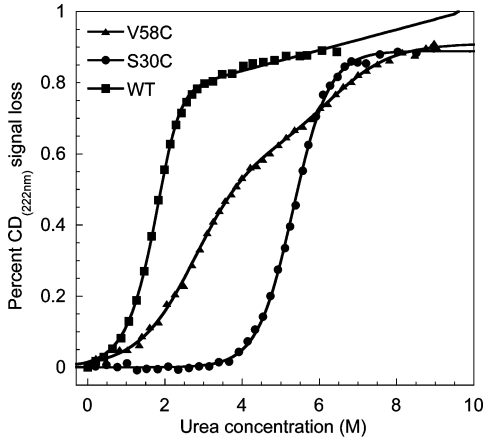

FIGURE 4: CD-monitored urea denaturations of WT FIS and the oxidized form of V58C and S30C at pH 4. WT and S30C data were fit to $N_2 \leftrightarrows U_2$ whereas the V58C was fit to the pathway $N_2 \leftrightarrows I_2 \leftrightarrows U_2$ because of the clear intermediate. Experiments were done with 1.8 μM FIS in 20 mM phosphate buffer and 0.1 M NaCl. Data were normalized as in Figure 2.

Table 4: Analysis of the Urea-Induced Equilibrium Denaturation of WT FIS and the Oxidized Cysteine Mutants at pH 4.0[a]

protein	ΔG (kcal/mol)	m [kcal/(mol·M)]	fit to the unfolding pathway
WT	11.8 ± 0.1	2.4 ± 0.1	$N_2 \leftrightarrows U_2$
V58C	6.1 ± 1.0	1.5 ± 0.2	$N_2 \leftrightarrows I_2 \leftrightarrows U_2$
S30C	6.7 ± 0.3	1.2 ± 0.1	$N_2 \leftrightarrows U_2$

[a] Oxidized V58C denaturation via GuHCl yielded an obvious three-state denaturation mechanism, and thus it was possible to fit the single denaturation curve to a three-state ($N_2 \leftrightarrows I_2 \leftrightarrows U_2$) mechanism. The results for each transition were resolved. For $N_2 \leftrightarrows I_2$, $\Delta G = 2.1$ kcal/mol and m-value = 0.9 kcal/(mol·M), and for $I_2 \leftrightarrows U_2$, $\Delta G = 3.9$ kcal/mol and m-value = 0.7 kcal/(mol·M). Errors are the standard deviations based on three independent experiments.

Urea-Induced Denaturation of Oxidized V58C FIS at pH 4 Results in a GuHCl-Like Denaturation Transition. The existence of an intermediate in the urea denaturation pathway of oxidized V58C FIS was supported by the results obtained by carrying out the denaturation at pH 4.0 (Figure 4). The urea denaturation of V58C FIS at pH 4 resulted in the decoupling of two transitions. Interestingly, S30C FIS did not show any shift to a biphasic urea denaturation at pH 4.0, but its m-value was reduced by over 20% compared with that at pH 7 (Table 4). In contrast, the m-value of WT FIS was not altered at pH 4.0. The decrease in m-value of S30C FIS suggests that there may be a hidden intermediate that is marginally populated at low pH. The shift in urea denaturation m-value with changing pH has been studied before, and a mathematical model has been proposed to explain how the presence of intermediates may result in m-value changes (*26*). It was shown that the pK_a's of the denaturation intermediates and native states dictate whether the m-value

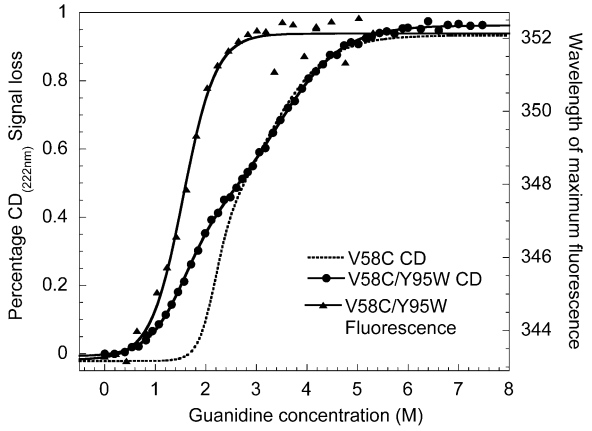

FIGURE 5: Comparison between fluorescence and CD-monitored GuHCl denaturation of oxidized FIS mutant V58C/Y95W. The dashed line represents the three-state fit to the CD monitored GuHCl denaturation of oxidized V58C presented in Figure 3, while the same pathway is used to fit the CD-monitored denaturation of V58C/Y95W here. Fluorescence monitored denaturation of V58C/Y95W is fit to the two-state mechanism ($N_2 \leftrightarrows I_2$). The resulting curve fit parameters for the $N_2 \leftrightarrows I_2$ transitions of V58C/Y95W monitored by CD and fluorescence are as follows: $\Delta G = 2.5$ kcal/mol and *m*-value = 1.6 kcal/(mol·M); $\Delta G = 2.5$ kcal/mol and *m*-value = 1.6 kcal/(mol·M), respectively. The parameters for the V58C/Y95W $I_2 \leftrightarrows U_2$ transition monitored by CD are $\Delta G = 3.2$ kcal/mol and *m*-value = 1.0 kcal/(mol·M). The CD data in this figure were normalized as explained in the Figure 2 legend, whereas raw fluorescence data is shown with correspondence to the right-hand *y*-axis.

increases or decreases with pH during urea denaturation (*26*). In the case of the cross-linked FIS mutants, the intermediates must have a pK_a that is closer to the unfolded state resulting in a smaller *m*-value at pH 4.0 than at pH 7.4.

Denaturation of Oxidized V58C/Y95W FIS Shows That the Intermediate Has a Disrupted C-Terminus. A double FIS mutant containing V58C and a tryptophan probe at position 95 (Y95W) was constructed to selectively monitor via fluorescence the denaturation of the DNA-binding subdomain (C and D helices, Figure 1) and test the hypothesis that the low denaturation cooperativity results from a loss of structure in this region. The GuHCl-induced denaturation of V58C/Y95W FIS was monitored by measuring the changes in the wavelength of maximum fluorescence (Figure 5). The results clearly show a denaturation transition that overlays only with the first of the two transitions observed in the V58C FIS GuHCl denaturation experiments monitored by CD (Figure 5). In contrast, the GuHCl-induced denaturation of V58C/Y95W monitored by CD exhibited two transitions. However, the low-denaturant transition was destabilized, which is consistent with the slight destabilization also noticed in a FIS variant carrying only the Y95W mutation (unpublished data). Thus, our ability to separately monitor the low denaturant transition in Y95W/V58C suggests that the first transition in V58C FIS is due to the unfolding of the C-terminus.

DISCUSSION

Effects of V58C and S30C Mutations on Structure, Stability, and DNA Binding. The negligible and negative effects on FIS stability of the reduced S30C and V58C, respectively, are consistent with Ser30 being largely solvent exposed and Val58 being buried in the hydrophobic core (Figure 1). Despite the decrease in stability, reduced V58C FIS exhibited native-like secondary structure and no reduction in DNA binding affinity compared with the WT FIS. Notwithstanding the large decrease in hydrophobicity, it is possible that the overall modest effect of the V58C FIS mutation may be due in part to the similarly low α helical propensities of valine and cysteine residues, together with the relatively moderate reduction (18%) in the van der Waals volume upon mutation.

When the Cys30 and Cys58 were oxidized, there was a large increase in the stability of FIS against urea- and GuHCl-induced denaturation. Since direct comparison between the ΔG of monomeric and dimeric proteins is not meaningful due to their different molecularity (*27*), the stabilizing effect of the C30−C30 and C58−C58 disulfide bond may be best quantified by determining their effect on the C_m. Compared with WT FIS, in oxidized S30C and V58C FIS there was a dramatic increase in the C_m of about 4.5 and 3.0 M urea, respectively. Thus, the formation of the disulfide bond C58−C58 more than compensated for the inherent destabilization of the V58C mutation, without adversely affecting the structure and DNA binding affinity. The close ΔG's of the cross-linked S30C and V58C FIS mutants determined in GuHCl denaturation further support this observation. Due to the much lower ΔG and *m*-value obtained for oxidized V58C FIS in urea and the clear biphasic three-state denaturation in GuHCl, we conclude that this value (6.7 kcal/mol, Table 3) is unreliable and suggests the presence of an intermediate despite the two-state-like transition in urea. Thus, the C58−C58 disulfide results in a protein that is more stable than WT and an equilibrium denaturation transition that is less cooperative than either WT or S30C.

Previous work estimated the K_d for the dissociation of FIS dimers to monomers to reside within a range from 10^{-8} to 10^{-7} M (*28*, *29*). On the other hand, we have seen that specific FIS−DNA binding in vitro occurs with an estimated K_d in the range from 10^{-11} to 10^{-9} M (Table 1 and ref *19*). This suggests that specific DNA binding occurs at FIS concentrations in which the dimeric state is poorly populated. However, our observations suggest that the stability of homodimeric FIS is not a limiting factor in its DNA binding affinity in vitro. Despite the contrasting effects of reduced S30C and V58C on the stability of FIS, both mutants showed moderate improvements in their specific DNA binding affinities compared with the WT FIS. Whereas the oxidized forms of S30C and V58C both exhibited a substantial increase in stability, their DNA binding affinities were roughly comparable to those of their reduced counterparts. While this demonstrates that preformed FIS dimers in solution are fully competent for specific DNA binding in vitro, it does not rule out the possibility that monomeric FIS may also be able to interact with DNA wherein dimers may be subsequently formed and stabilized. The availability of S30C and V58C mutants will serve as a valuable tool to test these models further.

Denaturation Cooperativity Breaks Down in Oxidized V58C FIS, Resulting in a Dimeric Intermediate with a Disrupted C-Terminus. The biphasic denaturation transition of oxidized V58C FIS in the presence of GuHCl or in urea at pH 4.0 suggests the presence of a denaturation intermediate with a disrupted C-terminus, which in the native state is mostly stabilized by a salt-bridge/hydrogen bond network

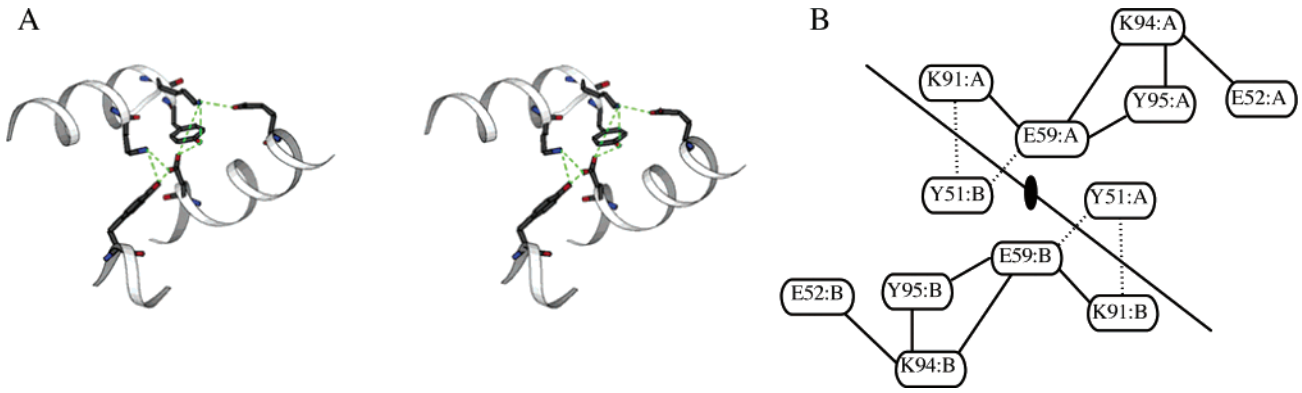

FIGURE 6: Diagram of the hydrogen bonding/salt-bridge network involving the B and D helices: (A) stereoview of the B and D helices based on the FIS structure 1FIA (*48*) and drawn using MOLSCRIPT (*52*); (B) schematic representation of the electrostatic network, where each residue is labeled with "A" and "B" to indicate the specific subunit to which it belongs. Inter- and intramolecular interactions are designated by dashed and solid lines, respectively. The six residues highlighted in panel A are represented in the same orientation in the illustration (panel B). The long diagonal solid line separates the two FIS subunits, and the symmetry axis is shown by an oval. The figure was reproduced with permission from ref *30*. Copyright 2004 American Chemical Society.

involving helices B and D (Figure 6) (*30*). To directly probe the conformational changes occurring at the C-terminus, we made a Y95W mutation onto V58C FIS. The GuHCl-induced denaturation of the oxidized double mutant V58C/Y95W FIS provided compelling evidence that that unfolding of the C-terminus was largely responsible for the first transition observed in disulfide cross-linked V58C FIS (Figure 5).

The nearly 60% loss of α helical signal in the first GuHCl denaturation transition of oxidized V58C FIS suggests that the conformational change that gives rise to the intermediate must involve more than the loss of structure at the C and D helices. The crystal structure of WT FIS shows that the small C and D helices of FIS dock against the B helix, involving mostly intra-subunit interactions. In addition, the C-terminal end of the C helix butts end-on-end with the N-terminus of the B helix of the opposite chain, basically capping the ends of the two helices via intermolecular hydrogen bonding (Figure 1). Since both ends of the B helices form intricate contacts with the C and D helices in FIS, it is likely that both ends of the B helix rely on structural stabilization conferred by the C and D helices. Thus, we speculate that in addition to the C and D helices, part of both ends of the B helix may unfold cooperatively to form the equilibrium intermediate observed in oxidized V58C FIS. Although a conformational change in the A helices cannot be ruled out, it seems likely that these helices are not disrupted in the intermediate since they do not interact with the C and D helices.

Structural and Energetic Basis for the Effect of Disulfide Bond Location on the Denaturation Cooperativity of FIS. The high cooperativity of the equilibrium denaturation transition of a protein arises from the co-dependent stabilization of its various structural regions (e.g., subdomains). Structural co-dependency implies that structural stabilization is transferred or shared between protein segments. Therefore, mutations may affect the denaturation cooperativity of a protein by affecting the stability of an individual segment or by affecting the efficiency with which stabilization energy is transferred throughout the protein. For a hypothetical protein with two subdomains, X and Y, that share an interface, there are two clear types of co-dependent structures. In one scenario, X could fold independently in the absence of Y, albeit with less stability, while Y would not fold at all in the absence of X. Here, a decrease in denaturation cooperativity might result if a mutation significantly stabilizes X but weakens the interaction between the two subdomains. In the second scenario, X and Y would not fold independently, yet together they may form a stable structure. In this case, both domains are likely to experience the effects of a mutation regardless of its location due to the large degree of sharing of stabilizing interactions. WT FIS resembles this latter scenario, as suggested by its two-state denaturation and the lack of structure in peptide models (comprising helices A, B, C + D, A + B, or B + C + D) of various combinations of FIS secondary structure (unpublished results). The C and D helices of FIS are short and packed against the B helices, and therefore, they depend on the rest of the protein for structural stability. This information suggests that the A/B helices and the C/D helices are structurally and energetically co-dependent, deriving a significant amount of their native stability from their intra- and intermolecular interactions with each other.

In oxidized V58C FIS, there is a nonuniform stabilization phenomena in which the disulfide bond significantly stabilizes the dimer core region (A and B helices) while having a lesser effect on the stability of the helix−turn−helix C-terminal subdomain. A similar effect, although less pronounced, was previously found for a P61A FIS mutation in the middle of helix B (*18*, *31*) that preferentially stabilized the A and B helices over the C/D helices (*32*). Similarly, the less cooperative transition of oxidized V58C FIS in GuHCl or at pH 4 in urea seems to be caused by selective stabilization of the A/B helices by the disulfide bond combined with the destabilization of the C-terminus via the disruption of the salt-bridge network by the GuHCl salt and low pH, thereby widening the stability gap between the two subdomains. In contrast, the disulfide bond in S30C FIS significantly stabilizes the protein but has a minimal effect on the cooperativity of denaturation. Since the S30C FIS mutation does not directly stabilize the B helices, the result is preservation of co-dependent stability of the B, C, and D helices. Consequently, the denaturation cooperativity is conserved and not significantly compromised by low pH or GuHCl.

General Insight about the Formation of Denaturation Intermediates. The propensity for the formation of equilib-

rium denaturation intermediates can be explained on the basis of the nonpolar character of the surface area exposed upon intermediate formation (*33*−*36*). In connection with partial protein unfolding (N ⇆ I*), surface area is exposed along the unfolded segment (US), as well as along the folded segment (FS), of the intermediate. While the solvent exposure of the nonpolar surface area along the US is entropically compensated by the dynamics of the unfolded structure, the nonpolar surface along the FS has no such energetic compensation. The exposure of nonpolar surface area along the FS, therefore, is the main factor that promotes denaturation cooperativity by destabilizing intermediates. In contrast, a low percentage of hydrophobic surface area buried at the interface between domains could signify a high probability for stable intermediate formation. Upon removal of the C and D helices (residues 71−98) from the crystal structure coordinates of WT FIS, the percentage of total nonpolar surface area increases from 48% to 53%, and the percentage of exposed backbone surface area that is nonpolar decreases from 45% to 41%. Although there is a small increase in hydrophobic surface area, the hydrophobic backbone is actually more buried in the model of the partially unfolded intermediate (residues 27−70) than in the full-length native state. The modest increase in overall exposure of hydrophobic surface area and the decrease in the percentage of the nonpolar backbone correlate well with the prediction that such a protein would be prone to intermediate formation. A viable hypothesis to draw from FIS and the treatment of equilibrium intermediates in the literature (*33*−*36*) is that hydrophobic, rather than polar, interfaces provide greater unfolding cooperativity and more efficient propagation of stability between domains. Thus it is logical to extend the hypothesis that mutagenic stabilization of the newly exposed folded surface area upon intermediate formation could favor the formation of an intermediate structure. This appears to be the case for V58C FIS, which directly cross-links the local structure that becomes exposed upon unfolding to the intermediate state, whereas S30C is not at all involved in such surface area.

Implications for Using Engineered Disulfide Bonds To Stabilize Protein Structure. This study has shown that the engineering of a disulfide bond can increase protein stability and still have a significant impact on the denaturation cooperativity. Although the addition of a disulfide bond stabilized the dimeric Arc repressor (*17*) and λ repressor (*15*) proteins without disrupting the denaturation cooperativity, intermediate formation is common in monomeric proteins with engineered disulfide bonds (*1*, *4*, *8*, *12*−*14*). If the goal is to stabilize a protein, the effect of engineered disulfide bonds on protein cooperativity may not be relevant. However, in cases where kinetic stability may be an important prerequisite, for example to avoid aggregation (*37*, *38*) or to allow a protein to withstand severe conditions (*39*), it may be necessary to thermodynamically stabilize a protein without compromising its folding cooperativity. Although protein kinetic stability and folding cooperativity are far from the same concept, both factors have been shown to reduce the probability of sampling partially unfolded states under native state conditions (*18*, *31*, *40*). With the goal of increasing stability, researchers have had the rare success of kinetically and thermodynamically stabilizing a thermolysin-like protease (*41*−*43*) via engineered disulfide bonds. The G8C/N60C mutant of this thermolysin-like protease resulted in a disulfide bond that introduced kinetic stability not present in the WT protein (*43*, *44*). This suggests that the disulfide bond caused an increase in the unfolding cooperativity and thus supports the assertion that high unfolding cooperativity is necessary for large kinetic stability. Therefore, engineering increased thermodynamic stability while maintaining folding and unfolding cooperativity is a potentially important step toward achieving kinetic stability.

Although some applications may call for a uniformly stable protein, it is known that preservation of unevenly distributed stability and flexibility may be important for proteins that have multiple functional domains with different stability requirements. Uneven distribution of stability and flexibility is in part responsible for the long-range propagation of signals from ligand binding sites, while low conformational stability in binding sites allows for high-affinity binding to low molecular weight ligands (*45*, *46*). The presence of low-stability regions at binding sites allows for fluctuation between binding-competent and binding-incompetent conformations and often constrains the population of binding-competent active sites to account for a small percentage of the native ensemble (*45*, *46*). As a result of having a majority population of binding-incompetent active sites, the binding of a ligand results in long-range conformational changes and a redistribution of populations among the native ensemble (*45*−*47*). FIS−DNA binding is accompanied by the bending of DNA (*48*). The C-terminal helix−turn−helix region interacts with DNA, while the N-terminal region of FIS stimulates Hin-mediated DNA inversion via interaction with the DNA-bound Hin recombinase. Interactions between FIS and the Hin recombinase are not observed in solution and require their association with specific DNA binding sites (*49*). Structural signals are likely to propagate through FIS, starting at the DNA-binding C-terminus, to affect the binding and bending of DNA and enable the N-terminus to associate with recombinase proteins.

Engineered disulfide bonds that stabilize protein structure usually involve conservative mutations that do not induce strain or remove favorable interactions. However, the former requirement appears to be much more important than the latter one, since the disulfide bond may compensate for the loss of stability caused by the deletion of an important interaction. The results of our study illustrate this point well since the C58−C58 disulfide bond compensates for the inherently destabilizing effect of the V58C mutation, thereby demonstrating that it is acceptable to engineer a disulfide bond by substituting buried hydrophobic residues for cysteines. Interestingly, even when the α carbons may appear to be out of range, this may not prevent the engineering of a stabilizing disulfide bond because the plasticity or dynamics of the disulfide bonded regions will be the main factor determining whether strain is imparted on the protein. Perhaps this is the reason a popular automated disulfide design algorithm (*50*) was unable to identify either disulfide bond created in this study, even when bond angle tolerance was at its maximum. Thus, it appears that the main criterion for engineering a stabilizing disulfide bond is to choose residues with side chains that are facing each other and α carbons that are at a distance of 7−8 Å. Furthermore, our results show that whereas conservative (e.g., serine for cysteine) mutations are ideal, even nonconservative (e.g.,

valine for cysteine) ones could lead to the successful engineering of a disulfide bond, although perhaps at the expense of folding cooperativity.

ACKNOWLEDGMENT

We thank Marta Manning for her helpful comments.

REFERENCES

1. Betz, S. F., and Pielak, G. J. (1992) Introduction of a disulfide bond into cytochrome *c* stabilizes a compact denatured state. *Biochemistry 31*, 12337−12344.
2. Betz, S. F. (1993) Disulfide bonds and the stability of globular proteins. *Protein Sci. 2*, 1551−1558.
3. Chau, M. H., and Nelson, J. W. (1992) Cooperative disulfide bond formation in apamin. *Biochemistry 31*, 4445−4450.
4. Clarke, J., and Fersht, A. R. (1993) Engineered disulfide bonds as probes of the folding pathway of barnase: increasing the stability of proteins against the rate of denaturation. *Biochemistry 32*, 4322−4329.
5. Doig, A. J., and Williams, D. H. (1991) Is the hydrophobic effect stabilizing or destabilizing in proteins? The contribution of disulphide bonds to protein stability. *J. Mol. Biol. 217*, 389−398.
6. Wetzel, R., Perry, L. J., Baase, W. A., and Becktel, W. J. (1988) Disulfide bonds and thermal stability in T4 lysozyme. *Proc. Natl. Acad. Sci. U.S.A. 85*, 401−405.
7. Wells, J. A., and Powers, D. B. (1986) In vivo formation and stability of engineered disulfide bonds in subtilisin. *J. Biol. Chem. 261*, 6564−6570.
8. Villafranca, J. E., Howell, E. E., Oatley, S. J., Xuong, N. H., and Kraut, J. (1987) An engineered disulfide bond in dihydrofolate reductase. *Biochemistry 26*, 2182−2189.
9. Tamura, A., Kojima, S., Miura, K., and Sturtevant, J. M. (1994) Effect of an intersubunit disulfide bond on the stability of Streptomyces subtilisin inhibitor. *Biochemistry 33*, 14512−14520.
10. Saunders, A. J., Young, G. B., and Pielak, G. J. (1993) Polarity of disulfide bonds. *Protein Sci. 2*, 1183−1184.
11. Flory, P. J. (1956) Theory of elastic mechanisms in fibrous proteins. *J. Am. Chem. Soc. 78*, 5222−5235.
12. Pace, C. N., Grimsley, G. R., Thomson, J. A., and Barnett, B. J. (1988) Conformational stability and activity of ribonuclease T1 with zero, one, and two intact disulfide bonds. *J. Biol. Chem. 263*, 11820−11825.
13. Matsumura, M., Becktel, W. J., Levitt, M., and Matthews, B. W. (1989) Stabilization of phage T4 lysozyme by engineered disulfide bonds. *Proc. Natl. Acad. Sci. U.S.A. 86*, 6562−6566.
14. Matsumura, M., and Matthews, B. W. (1989) Control of enzyme activity by an engineered disulfide bond. *Science 243*, 792−794.
15. Sauer, R. T., Hehir, K., Stearman, R. S., Weiss, M. A., Jeitler-Nilsson, A., Suchanek, E. G., and Pabo, C. O. (1986) An engineered intersubunit disulfide enhances the stability and DNA binding of the N-terminal domain of lambda repressor. *Biochemistry 25*, 5992−5998.
16. Regan, L., Rockwell, A., Wasserman, Z., and DeGrado, W. (1994) Disulfide cross-links to probe the structure and flexibility of a designed four-helix bundle protein. *Protein Sci. 3*, 2419−2427.
17. Robinson, C. R., and Sauer, R. T. (2000) Striking stabilization of Arc repressor by an engineered disulfide bond. *Biochemistry 39*, 12494−12502.
18. Hobart, S. A., Meinhold, D. W., Osuna, R., and Colon, W. (2002) From two-state to three-state: Effect of P61A mutation on the dynamics and stability of the factor for inversion stimulation results in an altered equilibrium denaturation mechanism. *Biochemistry 41*, 13744−13754.
19. Feldman-Cohen, L. S., Shao, Y., Meinhold, D., Miller, C., Colon, W., and Osuna, R. (2006) Common and variable contributions of Fis residues to high-affinity binding at different DNA sequences. *J. Bacteriol. 188*, 2081−2095.
20. Pace, C. N., Vajdos, F., Fee, L., Grimsley, G., and Theronica, G. (1995) How to measure and predict the molar absorption coefficient of a protein. *Protein Sci. 4*, 2411−2423.
21. Park, Y. C., and Bedouelle, H. (1998) Dimeric tyrosyl-tRNA synthetase from *Bacillus stearothermophilus* unfolds through a monomeric intermediate. A quantitative analysis under equilibrium conditions. *J. Biol. Chem. 273*, 18052−18059.
22. Myers, J. K., Pace, C. N., and Scholtz, J. M. (1995) Denaturant *m* values and heat capacity changes: Relation to changes in accessible surface areas of protein unfolding. *Protein Sci. 4*, 2138−2148.
23. Yuan, H. S., Finkel, S. E., Feng, J. A., Kaczor-Grzeskowiak, M., Johnson, R. C., and Dickerson, R. E. (1991) The molecular structure of wild-type and a mutant Fis protein: relationship between mutational changes and recombinational enhancer function or DNA binding. *Proc. Natl. Acad. Sci. U.S.A. 88*, 9558−9562.
24. Kostrewa, D., Granzin, J., Stock, D., Choe, H. W., Labahn, J., and Saenger, W. (1992) Crystal structure of the factor for inversion stimulation FIS at 2.0 Å resolution. *J. Mol. Biol. 226*, 209−226.
25. Thornton, J. M. (1981) Disulphide bridges in globular proteins. *J. Mol. Biol. 151*, 261−287.
26. Whitten, S. T., Wooll, J. O., Razeghifard, R., E, B. G., and Hilser, V. J. (2001) The origin of pH-dependent changes in m-values for the denaturant- induced unfolding of proteins. *J. Mol. Biol. 309*, 1165−1175.
27. Park, C., and Marqusee, S. (2004) Analysis of the stability of multimeric proteins by effective DeltaG and effective m-values. *Protein Sci. 13*, 2553−2558.
28. Hobart, S. A., Ilin, S., Moriarty, D. F., Osuna, R., and Colon, W. (2002) Equilibrium denaturation studies of the *E. coli* factor for inversion stimulation: implications for in vivo function. *Protein Sci. 11*, 1671−1680.
29. Topping, T. B., Hoch, D. A., and Gloss, L. M. (2004) Folding mechanism of FIS, the intertwined, dimeric factor for inversion stimulation. *J. Mol. Biol. 335*, 1065−1081.
30. Boswell, S. A., Mathew, J., Beach, M., Osuna, R., and Colón, W. (2004) Variable contributions of tyrosine residues to the structural and spectroscopic properties of the factor for inversion stimulation. *Biochemistry 43*, 2964−2977.
31. Meinhold, D., Boswell, S., and Colon, W. (2005) P61A mutation in the factor for inversion stimulation results in a thermostable dimeric intermediate. *Biochemistry 44*, 14715−14724.
32. Yuan, H. S., Wang, S. S., Yang, W.-Z., Finkel, S. E., and Johnson, R. C. (1994) The structure of Fis mutant $Pro^{61}Ala$ illustrates that the kink within the long α-helix is not due to the presence of the proline residue. *J. Biol. Chem. 269*, 28947−28954.
33. Murphy, K. P., Bhakuni, V., Xie, D., and Freire, E. (1992) The molecular basis of cooperativity in protein folding. III. Structural identification of cooperative folding units and folding intermediates. *J. Mol. Biol. 227*, 1143−1159.
34. Xie, D., and Freire, E. (1994) Molecular basis of cooperativity in protein folding. V. Thermodynamic and structural conditions for the stabilization of compact denatured states. *Proteins 19*, 291−301.
35. Freire, E., Murphy, K. P., Sanchez-Riuz, J. M., Galisteo, M. L., and Privalov, P. L. (1992) The molecular basis of cooperativity in protein folding. Thermodynamic dissection of interdomain interactions in phosphoglycerate kinase. *Biochemistry 31*, 250−256.
36. Freire, E., Haynie, D. T., and Xie, D. (1993) Molecular basis of cooperativity in protein folding. IV. CORE: a general cooperative folding model. *Proteins 17*, 111−123.
37. Lynch, S. M., Boswell, S. A., and Colon, W. (2004) Kinetic stability of Cu/Zn superoxide dismutase is dependent on its metal ligands: implications for ALS. *Biochemistry 43*, 16525−16531.
38. Lynch, S. M., and Colon, W. (2006) Dominant role of copper in the kinetic stability of Cu/Zn superoxide dismutase. *Biochem. Biophys. Res. Commun. 340*, 457−461.
39. Cunningham, E. L., Jaswal, S. S., Sohl, J. L., and Agard, D. A. (1999) Kinetic stability as a mechanism for protease longevity. *Proc. Natl. Acad. Sci. U.S.A. 96*, 11008−11014.
40. Jaswal, S. S., Sohl, J. L., Davis, J. H., and Agard, D. A. (2002) Energetic landscape of α-lytic protease optimizes longevitiy through kinetic stability. *Nature 415*, 343−346.
41. Mansfeld, J., Vriend, G., Dijkstra, B. W., Veltman, O. R., Van den Burg, B., Venema, G., Ulbrich-Hofmann, R., and Eijsink, G. H. (1997) Extreme stabilization of a thermolysin-like protease by an engineered disulfide bond. *J. Biol. Chem. 272*, 11152−11156.
42. Freire, E., and Murphy, K. P. (1991) Molecular basis of cooperativity in protein folding. *J. Mol. Biol. 222*, 687−698.
43. Durrschmidt, P., Mansfeld, J., and Ulbrich-Hofmann, R. (2005) An engineered disulfide bridge mimics the effect of calcium to protect neutral protease against local unfolding. *FEBS J. 272*, 1523−1534.

44. Durrschmidt, P., Mansfeld, J., and Ulbrich-Hofmann, R. (2001) Differentiation between conformational and autoproteolytic stability of the neutral protease from *Bacillus stearothermophilus* containing an engineered disulfide bond. *Eur. J. Biochem. 268*, 3612−3618.
45. Luque, I., and Freire, E. (2000) Structural stability of binding sites: consequences for binding affinity and allosteric effects. *Proteins* (Suppl 4), 63−71.
46. Luque, I., Leavitt, S. A., and Freire, E. (2002) The linkage between protein folding and functional cooperativity: two sides of the same coin? *Annu. Rev. Biophys. Biomol. Struct. 31*, 235−256.
47. Williams, D. C., Jr., Benjamin, D. C., Poljak, R. J., and Rule, G. S. (1996) Global changes in amide hydrogen exchange rates for a protein antigen in complex with three different antibodies. *J. Mol. Biol. 257*, 866−876.
48. Kostrewa, D., Granzin, J., Koch, C., Choe, H. W., Raghunathan, S., Wolf, W., Labahn, J., Kahmann, R., and Saenger, W. (1991) Three-dimensional structure of the *E. coli* DNA-binding protein FIS. *Nature 349*, 178−180.
49. Heichman, K. A., and Johnson, R. C. (1990) The Hin invertasome: protein-mediated joining of distant recombination sites at the enhancer. *Science 249*, 511−517.
50. Dombkowski, A. A. (2003) Disulfide by Design: a computational method for the rational design of disulfide bonds in proteins. *Bioinformatics 19*, 1852−1853.
51. Guex, N., and Peitsch, M. C. (1997) SWISS-MODEL and the Swiss-PdbViewer: an environment for comparative protein modeling. *Electrophoresis 18*, 2714−2723.
52. Kraulis, P. J. (1991) MOLSCRIPT: a program to produce both detailed and schematic plots of protein structures. *J. Appl. Crystallogr. 24*, 946−950.

BI060672N